

Quantification of methane sources in the Barnett shale (Texas) using the Penn State WRF-Chem-FDDA realtime modeling system

T. Lauvaux¹, Aijun Deng¹, Brian Gaudet¹, Colm Sweeney², Gabrielle Petron², Anna Karion², Alan Brewer³, Mike Hardesty³, Scott Herndon⁴, Tara Yacovitch⁴, Stephen Conley⁵

Abstract. Methane emissions from natural gas production areas are subject to large uncertainties at regional scales. Top-down methodologies offer an integrated approach to monitor these emissions but highly depend on the quality of the atmospheric model used to relate the surface emissions to the observed atmospheric concentrations. Using continuous measurements of in-situ CH₄ and C₂H₆ mixing ratios from an intensive aircraft campaign over the Barnett Shale area in March 2013, we evaluated the performance of the WRF-Chem modeling system using Four Dimensional Data Assimilation (FDDA) [Deng et al., 2012b] with World Meteorological Organization (WMO) surface stations and rawindsondes, aircraft meteorological measurements (wind, temperature, humidity), and vertical profiles of the mean horizontal wind from a Doppler Lidar. We show here that Mean Absolute Errors (MAE) of the direction and speed of the wind decreased with the assimilation of the additional aircraft and wind lidar data. However, the observed spatial variability across the domain suggests that several profilers or repeated aircraft transects are required to decrease significantly the MAE over the domain. Using our five WRF-FDDA simulations coupled to a Lagrangian Particle Dispersion Model (LPDM) [Uliasz, 1994], we evaluated the concentration footprints along the flight transect and quantified the sensitivity of the location and magnitude of the footprints to the meteorological fields. We show here that the WRF-FDDA-LPDM system is capable of distinguishing between the two major contributors to methane emissions in the area, i.e. from the urban area of Dallas-Fort Worth (DFW) and from the Barnett shale gas activities.

1. Introduction

Methane emissions from natural gas production areas are subject to large uncertainties at regional scales. Many measurements to date have focused on CH₄ mole fraction measurements, with no quantification of emissions (e.g. Phillips et al. [2013]). Measurements of fugitive emissions from gas production have focused primarily on measurements at the level of individual well pads, compressors, or even individual components of the plumbing within production facilities [US Office of Air Quality Planning and Standards US EPA, 1995]. This work has led to the creation of emissions factors which, when combined with activity data and extrapolated from a small number of one-time field measurements to tens of thousands of continuously operating well pads, provide existing emissions estimates. This approach is prone to systematic error, as emissions are highly variable

across production facilities and change over time with industry practice [Alvarez et al., 2012]. Large-area (10^4 km²) estimates from atmospheric greenhouse gas (GHG) measurements show great promise to address the shortcomings in existing shale gas emissions data. Aircraft missions have been used to document emissions from entire gas fields for limited periods of times (e.g., measurements over a single day). A single tower and mobile lab measurements were used in an emission ratio approach to estimate long-term emissions from drilling in the Denver-Julesburg basin of Colorado [Pétron et al., 2012]. This work also showed relatively large emissions ($\sim 4\%$ of production). We propose here to use simulated mesoscale meteorological variables instead of meteorological aircraft observations to compute the source-receptor relationship and quantify the emissions from gas production activities in the Barnett Shale area.

Top-down methodologies offer an integrated approach to monitor these emissions but highly depend on the quality of the atmospheric model used to relate the surface emissions to the observed atmospheric concentrations. Using continuous atmospheric measurements of in-situ methane and ethane mixing ratios from an intensive aircraft campaign over the Barnett Shale area in March 2013, we developed an atmospheric inversion system based on high resolution WRF simulations (1 km) and a Lagrangian Particle Dispersion Model (LPDM) [Uliasz, 1994] to invert for the methane sources in the area. We present here the performance of the WRF-FDDA modeling system [Deng et al., 2012a] using WMO surface stations and aircraft meteorological measurements (wind, temperature, humidity) compared to the initial WRF simulation in historical mode. We evaluated the impact of the additional aircraft data assimilated

¹Department of meteorology, The Pennsylvania State University, State College, PA

²The National Oceanic and Atmospheric Administration, Global Monitoring Division, Boulder, CO

³The National Oceanic and Atmospheric Administration, Chemistry M S, Boulder, CO

⁴Aerodyne Research Inc., Billerica, MA

⁵University of California at Davis, Davis, CA

in WRF-FDDA by using the concentration footprints along the different flight transects, and estimated the correlation between the locations of the footprints and the ethane-to-methane ratio of the sources. We finally discuss the modeling performance of our WRF-FDDA-LPDM system to distinguish the two major contributors to methane emissions in the area, i.e. from the urban area of Dallas-Fort Worth and from the Barnett shale gas activities.

2. Atmospheric modeling framework

2.1. WRF-Chem-FDDA

The WRF configuration for the model physics used for this study is the same as those used in Penn State NEXGEN airport forecast system (NGAFS, Deng et al. [2012b]), and is identical to the model physics in Rapid Refresh (RAP) and High Resolution Rapid Refresh (HRRR) systems used to provide short-range forecasts over North America. This configuration includes the use of: 1) the Thompson micro-physical processes, 2) the Grell 3-D ensemble scheme for cumulus parameterization on the coarse grid, 3) the Rapid Radiative Transfer Model (RRTM) for longwave atmospheric radiation, and the Dudhia scheme for shortwave atmospheric radiation, 4) the TKE-predicting Mellor-Yamada Level 2.5 turbulent closure scheme (MYJ PBL) for boundary layer turbulence parameterization, and 5) the 6-level RUC land surface model (LSM) for representation of the interaction between the land surface and the atmospheric surface layer. The initial and boundary conditions used in this study are based on the hourly 13-km RAP (initial) analysis fields that combine the latest satellite and radar observations.

The WRF modeling system also has four-dimensional data assimilation (FDDA) capabilities to allow the meteorological observations to be continuously assimilated into the model. The FDDA technique used in this study was originally developed for MM5 (Stauffer and Seaman 1994) and recently implemented into WRF [Deng et al., 2009]. It has several major uses. Firstly, it can be used to create four-dimensional dynamically consistent data sets or dynamic analyses (e.g., Deng et al. [2004]; Deng and Stauffer [2006]; Rogers et al. [2013]). Secondly, it can also be used to create improved lateral boundary conditions for process studies (e.g., Reen et al. [2006]). Finally, it can be used for dynamic initialization, where the model is relaxed towards observed conditions during a pre-forecast period to improve the initial state and the subsequent short-term forecast [Deng et al., 2012b]. The WRF model grid configuration used for this study is comprised of four grids: 9 km, 3 km and 1 km. The 9-km grid, with a mesh of 322x232 grid points, contains the most part of southwestern U.S. The 3-km grid, with a mesh of 202x202 grid points, contains part of Oklahoma and part of Texas. The 1-km grid, with a mesh of 202x202, only covers a small portion of northern Texas, similar to Figure 1. Fifty (50) vertical terrain-following layers are used, with the center point of the lowest model layer located \sim 12m above ground level (AGL). The thickness of the layers increases gradually with height, with 27 layers below 850 hPa (\sim 1550 m AGL). Note that WRF's vertical layers are defined based on the dry hydrostatic pressure and the height of the center point of each layer changes with time. The top of the model is set at 100 hPa. A one-way nesting strategy is used so that information from the coarse domains defines the lateral boundaries of the fine domains but no information from the fine domains feeds back to the coarse domains.

2.2. Lagrangian Particle Dispersion Modeling

The tracer backward transport was simulated here by the Lagrangian Particle Dispersion Model (LPDM) described by Uliasz [1994]. Particles are released from the receptors in a backward in time mode with the wind fields generated

by the eulerian model WRF-FDDA. In a backward in time transport mode, particles are released in LPDM from the measurement locations and travel to the surface and the boundaries. Compared to a forward mode, all the particles here are used to estimate fluxes, which reduces the computational cost of the simulation. The Lagrangian model LPDM was enhanced to simulate aircraft observations based on the precise trajectory of the airplane estimated by GPS (Global Positioning System). At each second, 5 particles are released at the position of the aircraft. A longer integration time would yield more particles and hence more reliable Lagrangian statistics but would misrepresent the aircraft trajectory. We use higher resolution for the aircraft measurement period because the eventual particle distributions are more sensitive to the explicitly resolved vertical velocity.

The dynamical fields in LPDM are forced by mean horizontal winds (u , v), potential temperature, and turbulent kinetic energy (TKE) from WRF-FDDA. At this resolution (1 km), turbulent motion corresponds to the closure of the energy budget at each time step. This scalar is used to quantify turbulent motion of particles as a pseudo random velocity. Based on the TKE, wind, and potential temperature, the Lagrangian model diagnoses turbulent vertical velocity and dissipation of turbulent energy. The off-line coupling between an Eulerian and a Lagrangian model solves most of the problems of non-linearity in the advection term at the mesoscale. Most of the non-linear processes resolved by the atmospheric model are attributed to a scalar representing the velocity of the particles. At each timestep (from one to 20 s), particles move with a velocity interpolated from the dynamical fields of the WRF-FDDA simulation (every 20 min). The timestep depends on the TKE, following the discretization described in Thomson (1987).

The formalism for inferring source-receptor relationships from particle distributions is described by Seibert and Frank [2004]. At each time step, the fraction of particles (released from one receptor at one time) within some volume, gives the influence of that volume on the receptor. If the volume includes the surface this will yield the influence of surface sources. If the volume includes the boundary (sides or top) it yields the influence of that part of the boundary.

3. GHG and meteorological measurements

3.1. Aircraft measurement campaign

In March and April 2013, an aircraft and ground-based mobile campaign was launched with the objective of quantifying methane fluxes from the Barnett Shale natural gas

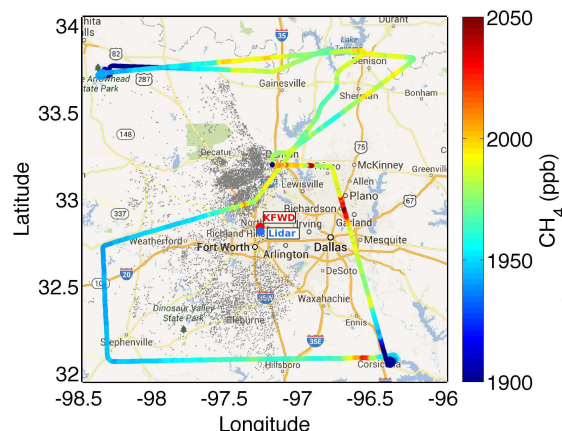


Figure 1. Map of the observed atmospheric methane (CH₄) mole fractions along the flight track for March 27, 2013 (in ppb). Natural gas well locations are indicated in gray.

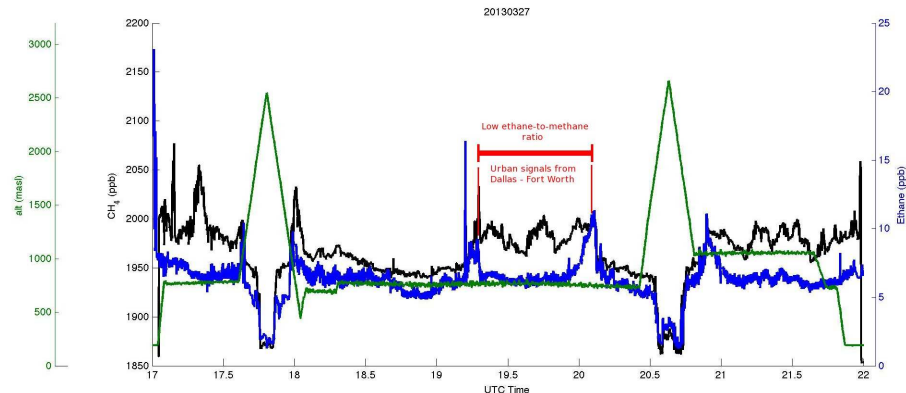


Figure 2. Time series of the observed atmospheric methane (in black) and ethane (in blue) mole fractions, and flight altitudes (in green) during the March 27, 2013 flight.

production field. A Mooney TLS-20 single engine aircraft (owned and operated by Scientific Aviation) was instrumented with a CRDS CO₂/CH₄/CO/H₂O (Picarro) analyzer measuring every 2.5 s (0.4 Hz) as well as an ethane (C₂H₆) analyzer (Aerodyne Inc.) at 1 Hz. Discrete flask air samples (NOAA/ESRL) were also collected on board. All instruments drew air from outside the aircraft from dedicated inlets installed under the starboard wing.

Five science flights were conducted in the Barnett region during clear weather conditions. Flight paths sampled air upwind and downwind of the gas field and the urban DFW area. The aircraft conducted two vertical profiles per flight to measure the mixing height of surface emissions. In this study, we simulated the meteorological conditions for one of the five flights of the campaign (March 27, 2013).

3.2. Meteorological measurements

The meteorological observations assimilated into the WRF-Chem-FDDA system are based on the WMO observations distributed by the National Weather Service (NWS), and include 2 hourly upper-air rawinsondes and 17 hourly surface observations, both within the fine mesh grid domain. In this study, two other meteorological data sets were available. The first data set includes temperature, moisture, and horizontal wind from the aircraft. The aircraft temperature was measured at 1 Hz from a Thermister mounted outside the aircraft. The water vapor measurements were made using the Picarro CRDS instrument at 0.4 Hz. The second set of measurements was collected by the High Resolution Doppler Lidar [Grund et al., 2001], measuring the horizontal mean wind, the vertical velocity variance, and the aerosol backscatter. For our application, we assimilated the horizontal mean wind every 20 minutes, available at a 30m vertical resolution in the first 3km of the atmospheric column. The different data sets were used alone or together, resulting in five different simulations of the meteorological conditions (cf. section 4.1). The aircraft data represent a large fraction of the domain compared to the rawinsonde and the HRDL, whereas the HRDL measures continuously the horizontal wind (averaged over 20-min intervals). The two data sets offer a higher density in space or in time, potentially impacting the atmospheric model along the simulations in different ways. We present in section 4.1 an evaluation of the modeling performances depending on the data sets used in the assimilation framework.

3.3. Source identification using ethane-to-methane gas ratios

Ethane is a component of raw gas, making it a good tracer for fugitive gas and oil-related emissions. CH₄ emissions from urban sources, such as landfills and wastewater treatment, have no correlated C₂H₆ emissions, as C₂H₆ is

not emitted by those sources. We present here the measurements for ethane (C₂H₆) and methane (CH₄) during one of the flights (March 27, 2013) (Fig. 2). The flight path offers a large coverage of the simulation domain (cf. Fig. 1), designed to sample the wide CH₄ plume in the area from both urban sources and gas production activities. In this figure, C₂H₆ and CH₄ measurements time series show three segments corresponding to enhanced CH₄ mixing ratios with no C₂H₆ enhancement. One segment of the flight was selected to define the influence of urban emissions in the observed CH₄ measurement time series. We selected the locations and time of the aircraft measurements with high CH₄ concentrations (>1,950ppb) synchronous with low ethane-to-methane ratios (3.05ppb_{C₂H₆}/ppm_{CH₄} instead of 3.13ppb_{C₂H₆}/ppm_{CH₄} for non-urban emissions), *i.e.* between 19.3 and 19.9 hours on March 27, which corresponds to one segment of the overall flight path. The particles released at the same times in LPDM correspond to these measurements, and can be tracked in time and space. The back trajectories of these particles, when touching the surface, should fit the extent of the urban area of Dallas-Fort-Worth. Using this technique, we can evaluate the performance of the WRF-Chem-FDDA model for the detection of urban emissions in the middle of the Barnett Shale gas production area. The results of this experiment are also valid for point source detection using mesoscale modeling at high resolution.

4. Results

4.1. Evaluation of the direct atmospheric transport (WRF-Chem-FDDA)

To evaluate the WRF model performance on the 1-km grid among the five experiments, mean absolute error (MAE) statistics for temperature, wind speed, and wind direction were computed to measure the model error. Sixteen surface stations, one upper-air sounding from Fort Worth (KFWD), and the Lidar mean horizontal wind, throughout the 48 hour period, between 12 UTC 26 March and 12 UTC 28 March 2013, were used in the meteorological evaluations. Comparison of the MAE time series of WRF-simulated surface wind speed and wind direction (temperature is not assimilated in the PBL) among the five experiments indicated that the added value of assimilating surface winds is evident (e.g. Fig. 3 (a)), since the surface wind direction MAE statistics are consistently improved in the FDDA experiments. For the upper-air statistics (e.g. Fig. 3 (b)), assimilation of WMO sonde data at KFWD substantially improved the WRF solutions for all three fields, since mass

fields along with winds were assimilated above the boundary layer; however, there was still more significant improvement in the wind fields, especially in wind direction (e.g., ~30 degree improvement in the lowest kilometer). Comparison between the FDDA (in green) and FDDA-w-Aircraft (in dark blue) shows that assimilating aircraft observations generally further improves the WRF simulation, but the improvement is not as significant as that of using WMO only. This is likely because the MAE is computed at the KFWD

location where the KFWD sonde is assimilated. Considering both FDDA simulations with the HRDL Lidar data at the KFWD site, the MAE increases around 1km a.g.l (Fig. 3 (b)). On the other hand, the MAE decreases significantly at the Lidar location when using the Lidar measurements (Fig. 3 (c), light blue and purple lines)). The two sites are distant by only few kilometers, with a difference in the observed wind speed of about 0.5 to 1 m/s. These results illustrate the spatial variability in the horizontal mean wind profiles across the domain. We discuss in section 5 the potential implications related to spatial variability and data assimilation in a mesoscale model.

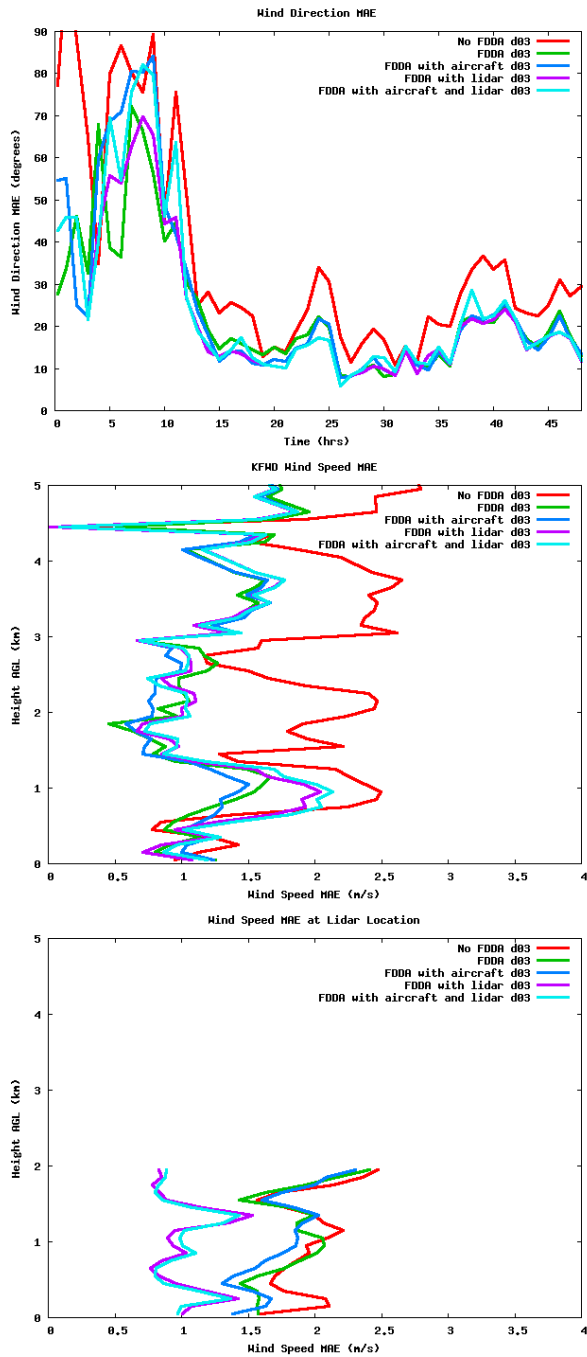


Figure 3. Mean absolute error for the 5 WRF-FDDA simulations for the wind direction for using 16 surface stations between 12 UTC 26 March and 12 UTC 28 March 2013 (upper panel), one vertical profile (KFWD) over the same period (middle panel), and the HRDL mean horizontal wind (lower panel).

4.2. Deconvolution of DFW city emission signals in the CH₄ backward plume

The particles released during the segment of the flight (on March 27, 2013) corresponding to the enhancement of CH₄ mole fractions but not C₂H₆ mole fractions were selected as a test-case for the detection of CH₄ city signals. The five WRF-Chem-FDDA simulations were coupled to the LPDM to generate footprints at the surface (cf. Fig. 4). These footprints were computed using the positions of the particles when close to the surface (50m high or lower), gridded at 1km resolution, and compared to the Dallas-Fort Worth urban area. In a perfect transport scenario, the cloud of particles near the surface should correspond exactly to the width of the urban area. Here, the spatial extent of the

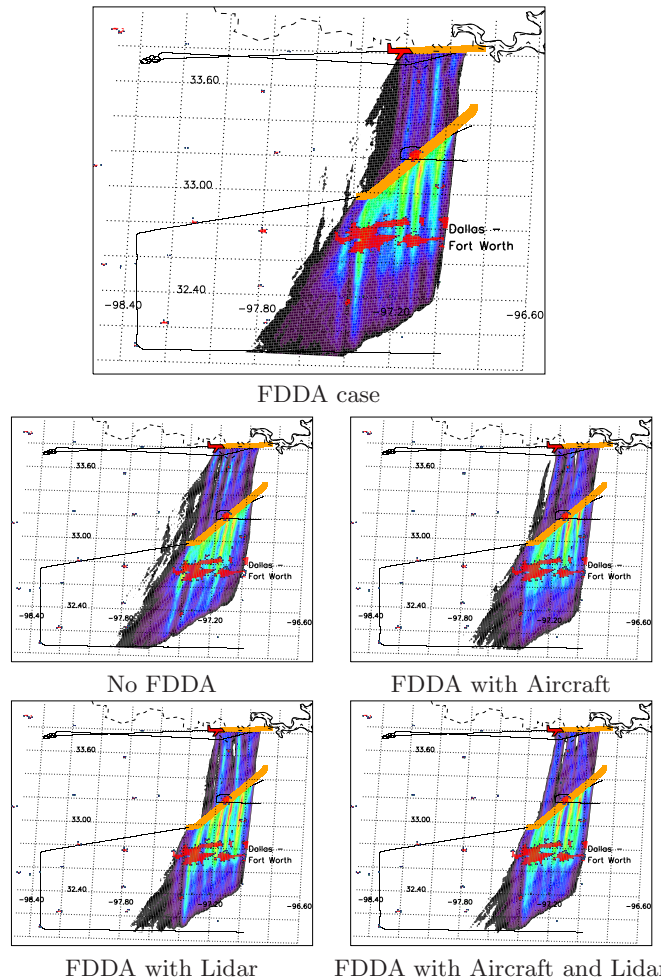


Figure 4. Maps of particles corresponding to low ethane to methane data

footprints, their amplitude and their orientation, reflect the impact of the meteorological driver data from WRF-Chem-FDDA, with some noticeable differences among them. This calculation would directly impacting a mass-balance calculation, combining our model results with the observed CH₄ concentrations. We show in Figure 4 that:

- The FDDA case footprint is aligned with the city limits, driven by a southern mean wind, and the spatial extent of the footprint to the South is about 32.6N, except one segment of the flight influenced by emissions further South.
- The no FDDA case (WRF in classic historical mode) shows that the footprint direction is biased toward the West and do not correspond exactly to the DFW urban area. The error in the wind direction would limit the potential use of the model results in the proper attribution of signals to the urban area. In addition, several sub-segments of the flight extend south of 32.6N.
- The FDDA-aircraft case shows a similar orientation of the footprints as the FDDA case, slightly shorter.
- the FDDA-Lidar case shows a larger amplitude with an enhanced sensitivity to the surface emissions, and an increased extent of one sub-segment to 32.2N.
- The FDDA-aircraft-Lidar footprint is narrower and despite a correct orientation (confirmed by the improvement in the wind direction in Fig. 3), the width of the footprint is under-estimated. However, the magnitude of the footprint remains unchanged (compared to the FDDA case).

The impact of the data assimilated in WRF-Chem shows that the density in time and space plays a critical role in constraining the footprint at the surface. Our five simulations show clear differences despite an overall agreement of the spatial distribution. We discuss in section 5 the impact of these differences for source detection and quantification.

5. Discussion and conclusions

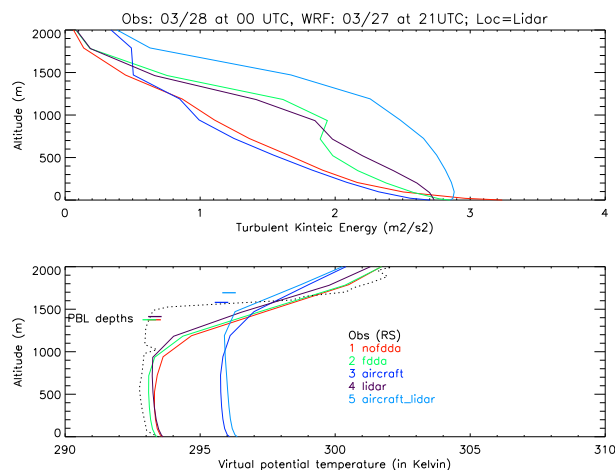


Figure 5. Simulated Turbulent Kinetic Energy (in $\text{m}^2 \cdot \text{s}^{-2}$) and Potential Temperature profiles from the five WRF simulations at 21 UTC (27 March 2013), and observed potential temperature (dashed line) at 00 UTC (28 March 2013)

Table 1. Difference (in %) to the mean surface footprint for the five simulations aggregated over the entire domain (first row) and for the urban area of Dallas-Fort-Worth (second row)

Case	No FDDA	FDDA	Aircraft	Lidar	Air+Lidar
Domain	2%	2.6%	-3.2%	1.7%	-3%
Urban	2.9%	-6.3%	-3.1%	3.5%	2.9%

We computed the footprints corresponding to the CH₄ emissions from the urban area of Dallas-Fort-worth by releasing particles at the exact GPS positions where low ethane-to-methane gas ratios were measured during the flight. As explained in section 3.3, the associated footprints should correspond to the urban area and can be used to evaluate the modeled surface footprints. Figure 4 shows the different surface footprints corresponding to the low ethane-to-methane ratios (cf. Fig. 2, period indicated in red). The differences in the wind direction between the FDDA and the no-FDDA simulations is clearly visible (Figure 4), as shown in Figure 3, with a shift in the orientation of the surface footprints. Considering the difference among the various FDDA cases, whereas the MAE did not show any significant impact, the spatial distribution of the surface footprints (and more specifically their lengths along the main wind direction) can vary significantly from one simulation to another. In a mass-balance approach, the variability in the surface footprints is propagated into the calculated CH₄ emissions and contribute to the overall uncertainty associated with the emission estimate. As noted in section 4.1, this variability in the footprints is related to the observed variability in space. These results suggest that a sufficient sampling density is necessary in order to improve the modeling results across the domain, which is critical for an aircraft campaign covering a large fraction of the fine mesh domain.

We present in Table 1 the impact of the different data sets used in the WRF-Chem-FDDA system on the amplitude of the surface footprints, for the urban area only and over the entire domain. The results indicate that the variability in the sensitivity to the surface emissions is about 10% for the urban area, and about 6% for the overall domain. In addition, the no-FDDA simulation produces similar estimates than other cases, within the range of the 4 FDDA cases despite the clear bias in the wind direction (cf. Fig. 3). The results suggest that the assimilation of meteorological data in our simulation do not constrain significantly the magnitude of the footprints. This magnitude is primarily driven by the mixing depth and the vertical mixing strength. In other terms, the physics of the WRF model (*i.e.* PBL scheme and Land Surface Model) drives the vertical mixing near the surface which limits the impact of the data assimilation on the mixing height. However, a recent study over the San Francisco bay area showed that the PBL depth can be slightly improved over longer time scales [Rogers et al., 2013].

We finally estimated the sensitivity to the PBL depths, directly impacting the magnitude of the surface footprints, which can be affected by the assimilation of observations within the PBL (wind fields only) and above the PBL (wind fields and temperature/moisture), as shown in Rogers et al. [2013]. We show in Figure 5 the profile of Turbulent Kinetic Energy (TKE) (upper panel) and the potential temperature (lower panel) for the five cases at 21UTC, 27 March 2013 at the exact location of the lidar. The observed potential temperature profile from the KFWD rawinsonde at 00UTC on 28 March is shown on the same plot (lower panel, dashed line). We also computed the PBL depths using the bulk Richardson number (lower panel) which uses the potential temperature vertical gradient. The assimilation of aircraft data (blue lines) increases the PBL depth at this location (lower panel), whereas the lidar alone or the initial FDDA cases do not impact the PBL depth. Considering the turbulent vertical mixing (upper panel), the TKE increases clearly when using the lidar data, but the impact of the aircraft data on the buoyancy term is unclear, which suggests that the increase in PBL depth is related to the shear production term in this case. The variability in the vertical mixing due to the assimilation of various data sets may explain some of the differences in the amplitude of the surface footprints, but no clear correlation between the sign of the difference (cf. Table 1) and the vertical mixing strength was observed.

Acknowledgments. This work was supported by the National Atmospheric and Oceanic Administration. Colm Sweeney, Anna Karion, Gabrielle Petron and Stephen Conley provided the aircraft measurements; Aijun Deng and Brian Gaudet performed the WRF-Chem-FDDA simulations; Alan Brewer and Mike Hardesty provided the HRDL Lidar data; and Scott Herndon and Tara Yacovitch helped with the calibration of the C₂H₆ Aerodyne analyzer.

References

- Alvarez, R. A., S. W. Pacala, J. J. Winebrake, W. L. Chameides, and S. P. Hamburg, 2012: Greater focus needed on methane leakage from natural gas infrastructure. *Proceedings of the National Academy of Sciences*, doi:10.1073/pnas.1202407109.
- Deng, A., , D. Stauffer, B. Gaudet, and G. Hunter, 2012a: A rapidly relocatable high-resolution WRF system for military-defense, aviation and wind energy. *WRF Users Workshop 2012, Boulder, CO*, 11pp.
- Deng, A., T. Lauvaux, K. Davis, N. Miles, S. Richardson, and D. Stauffer, 2012b: A WRF-Chem realtime modeling system for monitoring CO₂ emissions. *WRF Users Workshop 2012, Boulder, CO*, 6pp.
- Deng, A., N. Seaman, G. Hunter, and D. Stauffer, 2004: Evaluation of interregional transport using the MM5-SCIPUFF system. *J. of Applied Meteor.*, **43**, 1864–1886.
- Deng, A. and D. Stauffer, 2006: On improving 4-km mesoscale model simulations. *J. of Applied Meteor.*, **45**, 361–381.
- Deng, A., D. Stauffer, B. Gaudet, J. Dudhia, J. Hacker, C. Bruyere, W. Wu, F. Vandenbergh, Y. Liu, and A. Bourgeois, 2009: Update on wrf-arw end-to-end multi-scale fdda system. *WRF Users Workshop 2009, Boulder, CO*.
- Grund, C., R. Banta, J. George, J. Howell, M. Post, R. Richter, and A. Weickmann, 2001: High-resolution doppler lidar for boundary layer and cloud research. *Journal of Atmospheric and Oceanic Technology*, **18(3)**, 376–393.
- Pétron, G., G. Frost, B. R. Miller, A. I. Hirsch, S. A. Montzka, A. Karion, M. Trainer, C. Sweeney, A. E. Andrews, L. Miller, J. Kofler, A. Bar-Ilan, E. J. Dlugokencky, L. Patrick, C. T. Moore, T. B. Ryerson, C. Siso, W. Kolodzey, P. M. Lang, T. Conway, P. Novelli, K. Masarie, B. Hall, D. Guenther, D. Kitzis, J. Miller, D. Welsh, D. Wolfe, W. Neff, and P. Tans, 2012: Hydrocarbon emissions characterization in the colorado front range: A pilot study. *J. Geophys. Res.*, **117**, n/a–n/a, doi:10.1029/2011JD016360.
- URL <http://dx.doi.org/10.1029/2011JD016360>
- Phillips, N. G., R. Ackley, E. R. Crosson, A. Down, L. R. Hutyla, M. Brondfield, J. D. Karr, K. Zhao, and R. B. Jackson, 2013: Mapping urban pipeline leaks: Methane leaks across boston. *Environmental Pollution*, **173**, 1 – 4, doi:http://dx.doi.org/10.1016/j.envpol.2012.11.003.
- Reen, B., D. R. Stauffer, K. Davis, and A. R. Desai, 2006: A case study on the effects of heterogeneous soil moisture on mesoscale boundary-layer structure in the southern great plains, U.S.A. part ii: Mesoscale modelling. *Bound.-Layer Meteor.*, **120**, 275–314, doi:10.1007/s10546-006-9056-6.
- Rogers, R. E., A. Deng, D. R. Stauffer, B. J. Gaudet, Y. Jia, S.-T. Soong, and S. Tanrikulu, 2013: Application of the weather research and forecasting model for air quality modeling in the san francisco bay area. *J. Appl. Meteor. Climatol.*, **52(9)**, 1953–1973, doi:10.1175/JAMC-D-12-0280.1.
- Seibert, P. and A. Frank, 2004: Source-receptor matrix calculation with a lagrangian particle dispersion model in backward mode. *Atmospheric Chemistry and Physics*, **4**, 51–63, doi:10.5194/acp-4-51-2004.
- URL <http://www.atmos-chem-phys.net/4/51/2004/>
- Uliasz, M., 1994: Lagrangian particle modeling in mesoscale applications. *Environmental Modelling II*, P. Zanetti, ed., Computational Mechanics Publications, 71–102.
- US Office of Air Quality Planning and Standards US EPA, 1995: Compilation of air pollutant emission factors, volume 1: Stationary point and area sources, chapter 1.3: External combustion sources, fuel oil combustion. US EPA Tech. paper ap-42 5th edition, US EPA.

T. Lauvaux, Department of Meteorology, The Pennsylvania State University, 412 Walker Building, University Park, PA 16802, USA. (tul5@psu.edu)